Biomedicine & Pharmacotherapy 149 (2022) 112881

Contents lists available at ScienceDirect

Biomedicine & Pharmacotherapy

journal homepage: www.elsevier.com/locate/biopha

Tetralol derivative NNC-55-0396 induces glioblastoma cell death by activating IRE1α, JNK1 and calcium signaling

Anna Visa, Lía Alza, Carles Cantí *, Judit Herreros *

Cell Calcium Signaling Lab, IRBLleida, University of Lleida, Rovira Roure 80, 25198 Lleida, Spain

ARTICLE INFO

KEYWORDS:
Calcium
Glioblastoma
ER stress
Cell death

ABSTRACT

Mibefradil and NNC-55–0396, tetralol derivatives with a proven –ability to block T-type calcium channels in excitable cells, reduce cancer cell viability in vitro, causing cell death. Furthermore, they reduce tumor growth in preclinical models of Glioblastoma multiforme (GBM), a brain tumor of poor prognosis. Here we found that GBM cells treated with cytotoxic concentrations of NNC-55–0396 paradoxically increased cytosolic calcium levels through the activation of inositol triphosphate receptors (IP_3R) and ER stress. We used pharmacological inhibitors and gene silencing to dissect the cell death pathway stimulated by NNC-55-0396 in GBM cell lines and biopsy-derived cultures. Calcium chelation or IP_3R inhibition prevented NNC-55–0396-mediated cytotoxicity, indicating that ER calcium efflux is the cause of cell death. Upstream of calcium mobilization, NNC-55–0396 activated the IRE1α arm of the Unfolded Protein Response (UPR) resulting in the nuclear translocation of pro-apoptotic CHOP. Consistent with these findings, silencing *IRE1α* or *JNK1* rescued the cell death elicited by NNC-55–0396. Therefore, we demonstrate that activation of IRE1α and calcium signaling accounts for the cytotoxicity of NNC-55–0396 in GBM cells. The delineation of the signaling pathway that mediates the abrupt cell death triggered by this compound can help the development of new therapies for GBM.

1. Background

Disrupting the endoplasmic reticulum (ER)-protein folding capacity [1,2] is at the root of neurodegenerative diseases, diabetes and cancer. Indeed, cancer cells maintain high levels of protein synthesis and are exposed to a variety of intrinsic (including genomic instability and oncogene activation) and extrinsic (lack of nutrients or oxygen, exposure to chemo/radiotherapy) stresses.

The Unfolded Protein Response (UPR) is a cell signaling network adapted to respond to ER stress. Cancer cells show overactive UPR cascades that contribute to therapeutic resistance. Nevertheless, a sustained stimulation of the UPR can also trigger cell death [3]. The UPR consists of three branches: the IRE1α (Inositol Requiring Enzyme 1), PERK (PKR-like ER kinase) and ATF6 (Activating Transcription Factor 6) pathways. Calcium-dependent chaperone GRP78/BIP binds to misfolded proteins, if abundant, and sets the UPR sensors free for activation. Specifically, IRE1α/ERN is a Ser/Thr kinase that phosphorylates JNK (c-Jun N-terminal Kinase) to induce apoptosis, promotes the splicing of XBP1 (X-box Binding Protein 1) or degrades mRNAs through its RIDD (Regulated IRE-Dependent Decay) domain. Unbalanced or unmanageable ER stress stimulates the nuclear translocation of CHOP/GADD153, which governs the apoptotic response [4].

In addition to the UPR's adaptive role in cancer, it has been proposed that mutations in UPR components can drive tumorigenesis. IRE1α is one of the most mutated kinases in different cancers [5]. In glioblastoma multiforme (GBM), a fatal brain tumor, an IRE1α signaling signature associates with aggressiveness and poor prognosis [6,7]. Moreover, IRE1α plays antagonistic roles in GBM development through XBP1 and RIDD-dependent functions [6].

Voltage-gated calcium channels, best known for their roles in membrane excitability, are key transducers of membrane potential changes into signaling cascades. Particularly, T-type calcium channels (TTCCs) are widely expressed in non-excitable cells, in which they promote G1/S cell cycle transition [8,9]. TTCC expression in cancer cells

Abbreviations: 2-APB, 2-Aminoethoxydiphenyl borate; BAPTA-AM, 1,2-bis(2-aminophenoxy)ethane-N,N,N′,N′-tetraacetic acid tetrakis (acetpxymethyl ester); ER, endoplasmic reticulum; F, fluorescence; GBM, glioblastoma multiforme; IP_3R, inositol triphosphate receptors; NNC, NNC-55–0396; PBS, phosphate buffer saline; PI, propidium iodide; Tg, thapsigargin; TTCC, T-type calcium channels; UPR, Unfolded Protein Response; WST-1, (4-[3-(4-iodophenyl)-2-(4-nitrophenyl)–2H-5-tetrazolium]-1,3-benzene disulfonate; XeC, Xestospongin-C.

* Corresponding authors.
E-mail addresses: anna.visa@udl.cat (A. Visa), lia.alza@udl.cat (L. Alza), carles.canti@udl.cat (C. Cantí), judit.herreros@udl.cat (J. Herreros).

https://doi.org/10.1016/j.biopha.2022.112881
Received 29 January 2022; Received in revised form 11 March 2022; Accepted 23 March 2022
Available online 31 March 2022

warrants research on their value as prognostic markers and chemotherapeutic targets [13,14]. Tetralol derivatives, mibefradil and NNC-55–0396, stand up as potent TTCC blockers that have been used in patients to treat cardiovascular disorders. These compounds induce apoptosis in cancer cells in vitro [14,15] and delay tumor growth in preclinical models [16–18]. Thus, mibefradil was granted the orphan drug status and repurposed for cancer investigation [10]. In a phase II trial on recurrent GBM patients, co-administration of mibefradil and the standard chemotherapeutic temozolomide increased overall and progression-free survival of patients compared to the temozolomide group [16]. Remarkably, the concentrations at which reportedly tetralols exert cytotoxic effects on cultured cancer cells are markedly higher than those required to block TTCCs. Based on a systematic analysis of electrophysiological data, we proposed that the cancer cell death induced by tetralols was likely due to off-target actions [17].

Here we aimed at dissecting the molecular mechanisms by which NNC-55-0396, a mibefradil analog, triggers GBM cell death. Unexpectedly, we found that NNC-55-0396 increases cytosolic calcium and activates the IRE1α UPR branch that leads to an apoptotic response mediated by CHOP. By identifying the death pathway triggered by NNC-55-0396, we highlight UPR components and calcium-dependent signaling cascades that when overstimulated render GBM cells sensitive to apoptosis. These pathways could be exploited in cancer therapy.

2. Materials and methods

2.1. Reagents and antibodies

Reagents were from the following companies: thapsigargin from Merck Sigma-Aldrich (Darmstadt, Germany), xestospongin-C from Cayman Chemical (Ann Arbor, Michigan, USA), 2-APB from Santa Cruz Biotechnology (Dallas, Texas, USA), BAPTA-AM from BioVision (Milpitas, California, USA), NNC 55–0396 from Alomone (Jerusalem, Israel) and KN-62 from APExBIO Technology (Boston, Massachusetts, USA). WST-1 reagent was from Roche (Basel, Switzerland).

Antibodies used were: β-actin (Merck Sigma-Aldrich, New Jersey, USA; A5441), P-Ser724-IRE1α (Novus Biologicals, Missouri, USA; NB100–2323SS), total IRE1α (Cell Signaling Technology, Massachusetts, USA; 3294, 14C10), CHOP (Santa Cruz Biotechnology, Dallas, USA; sc-7351), P-Thr183/Tyr185-JNK (Cell Signaling Technology, Massachusetts, USA; 9251), P-Ser73-c-Jun (Cell Signaling Technology; 3270, D47G9), Ero1α (Cell Signaling Technology; 3264), JNK1 (Santa Cruz Biotechnology; sc-1648), P-Thr286-CaMKII (Abcam, Cambridge, UK; ab32678).

2.2. Cell culture

GBM cell lines were obtained from the American Tissue Culture Collection (ATCC) and maintained in Minimal Essential Medium (Thermo Fisher Scientific, Massachusetts, USA) containing 10% heat-inactivated foetal bovine serum (Thermo Fisher Scientific, USA, 10270098), penicillin/streptomycin (Thermo Fisher Scientific, USA), L-glutamine (Thermo Fisher Scientific, USA) and 1% non-essential aminoacids (Thermo Fisher Scientific, USA). U87-MG and A172 cell lines were authenticated by short tandem repeat profiling (StabVida, Portugal) following purification of genomic DNA using the Maxwell16 Tissue DNA kit (Promega, Madison, Wisconsin). Cell lines were grown in mycoplasma-free rooms and mycoplasma testing was performed by PCR (primers used were forward: GGCGAATGGGTGAGTAACACG and reverse: CGGATAACGCTTGCGACCTATG). Cells that tested positive were either discarded or treated with Plasmocin (Thermo Fisher Scientific ant-mpt-1). Cell lines were passaged for 20–25 passages.

Primary GBM cell cultures were established from surgical biopsies obtained from Hospital Arnau de Vilanova of Lleida (Spain) as described [18], following approval by the review board of the IRBLleida-Biobank and of the Ethical Committee of the University of Lleida (code 235/CEIC/2019). Cultures were grown in Dulbecco's Minimal Essential Medium (Lonza, BE12–741 F) containing 10% foetal bovine serum and penicillin/streptomycin.

2.3. Western blot

Cells were washed with phosphate buffer saline (PBS) and lysed in Tris 62.5 mM, pH = 6.8 and 2% SDS. Cell lysates were resolved in SDS-PAGE gels and transferred to a polyvinylidene diflouride membrane. Membranes were cut to probe different antibodies on the same membrane. Membranes were blocked with 5% bovine serum albumin or milk and incubated overnight with primary antibodies. Blots were developed using Enhanced Chemiluminescence (Thermo Fisher Scientific) or Luminata Forte Horseradish Peroxidase Substrate (Merck Millipore). Band intensity was measured using ImageJ software and normalized against β-actin.

2.4. Immunofluorescence

Cells were cultured on poly-D-lysine glass coverslips, fixed with 4% paraformaldehyde (15 min, room temperature), washed, blocked and permeabilized in PBS containing 5% foetal bovine serum, 5% horse serum (Gibco), 0.2% glycine, 0.1% Triton X-100 (Merck Sigma-Aldrich) before incubation with primary antibodies. Secondary antibodies coupled to Alexa Fluor-488 or Fluor- 594 were incubated together with Hoechst. Coverslips were mounted on Mowiol. Micrographs were obtained using an inverted Olympus IX70 microscope (10x, 0.3 NA or 10x, 0.4 NA) equipped with epifluorescence optics and a camera (Olympus OM-4 Ti). Images were acquired using DPM Manager Software. The intensity of CHOP nuclear immunostaining and the number of vacuoles were quantified using ImageJ.

2.5. shRNA-induced gene silencing

Lentiviral-based vectors for RNA interference-mediated gene silencing were pLKO.1-puro (Mission-RNA; Merck Sigma-Aldrich) containing shRNAs scrambled (against the sequence 5′ CAACAAGATGAAGAGCACCAA 3′), *IRE1α* (TRCN0000000529) or *JNK1* (TRCN0000001055). Lentiviral particles were produced in HEK293T cells for 72 h upon transfection of the shRNA vectors together with psPAX2 and pMD2G plasmids (a gift of Dr D. Trono, Lausanne, Switzerland) using polyenthyleneimine. Medium was centrifuged (1 000 x g, 5 min) and filtered (0.45 mm). Cells were incubated with medium containing lentiviral particles for 24 h (polybrene 1.75 mg/ml was added to enhance viral infection). Then, medium was replaced to allow the knockdown for 4 or more days. Puromycin (2 mg/ml) was added to the media to select for resistant cells.

2.6. Calcium measurements

Cytosolic calcium was measured using the Fluo-4 AM dye (AAT Bioquest, USA) according to the manufacturer's instructions. For each condition 30,000 cells were seeded on 96-well black plates previously coated with poly-D-lysine 30 μg/ml. One h before initial measurements, cells were washed with PBS and incubated with 50 μl Hank's Buffer with Hepes containing 2 μM of Fluo-4, 2.5 mM of probenecid (AAT Bioquest) and 0.04% pluronic acid (Pluronic® F-127, Thermo Fisher Scientific). Cells were cultured for 30 min at 37 °C. After an additional incubation for 30 min at room temperature, cells were washed with 150 μl of Hank's solution with probenecid and pluronic acid and placed in a Tecan Infinite M200 microplate reader (Tecan, Switzerland) for basal fluorescence intensity measurement. Cells were excited at 490 nm and Ca^{2+}-bound Fluo-4 emission was recorded at 520 nm. Then, cells were treated and transferred to the fluorimeter at the indicated times for readings (XeC and 2-APB were pre-incubated for 30 min). Fluorescence values (F) were obtained from triplicate wells, normalized to the basal

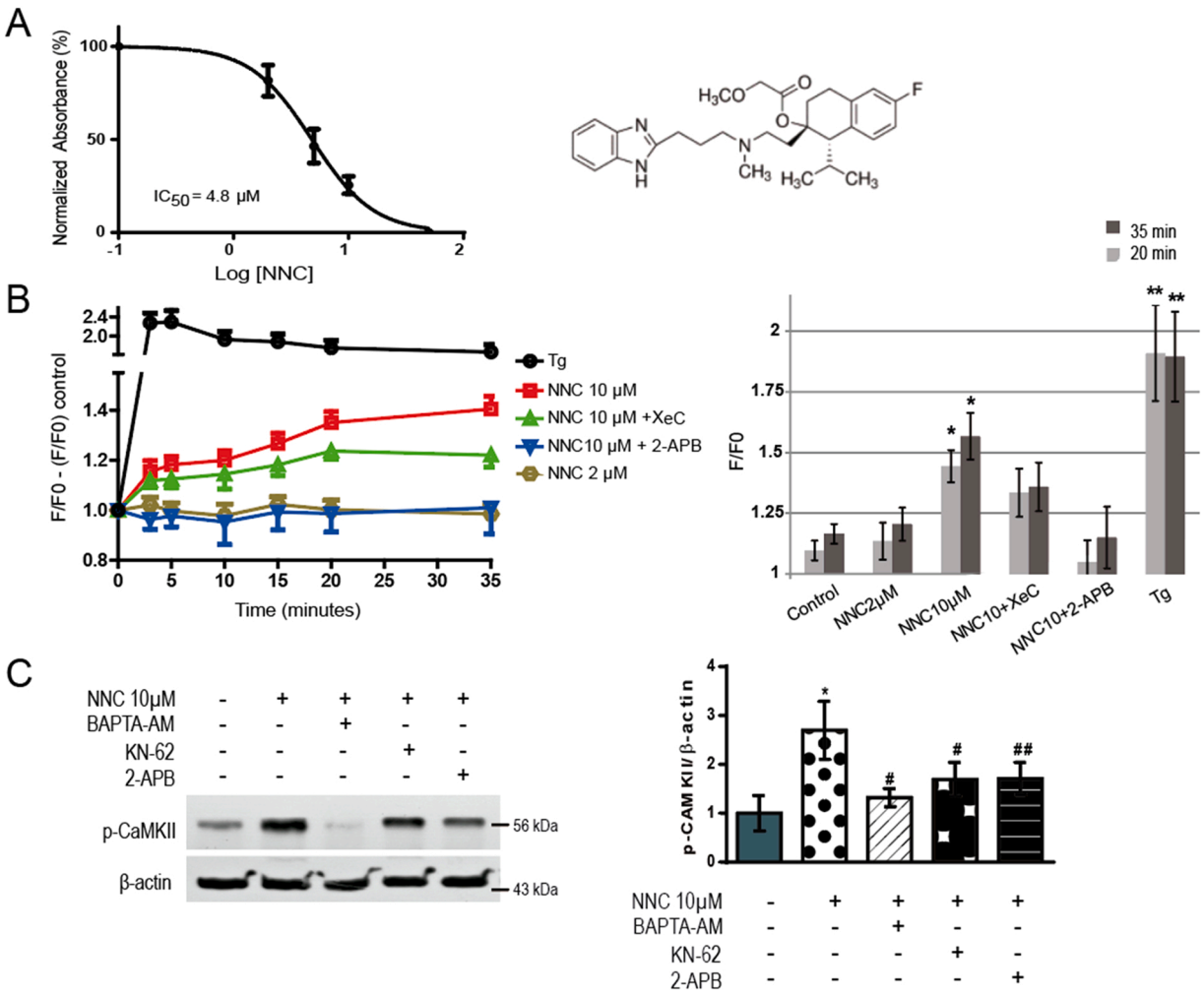

Fig. 1. NNC (10 µM) increases cytosolic calcium levels and activates CAMKII. A) Concentration dependence curve of normalized absorbance (representing % of A172 viable cells) plotted vs increasing concentrations of NNC (log scale). IC_{50} is indicated (n = 5). (Right) Molecular structure of NNC-55–0396. B) Cytosolic calcium levels were monitored using the Fluo-4 AM dye in A172 cells treated with 2 µM NNC or 10 µM NNC (alone or in combination with 40 µM 2-APB or 5 µM XeC). Co-administration of IP_3R antagonists, XeC and especially 2-APB, reduced the increase in cytosolic calcium levels triggered by 10 µM NNC. Tg (5 µM) was used as a positive control. Plot represents the ratio of fluorescence F/F_0 for the treatment (F_o, basal fluorescence intensity) subtracting the control F/F_0 (n = 3–11). Histogram (right) represents the ratio F/F_0 for the different conditions at 20 and 35 min. Data were analyzed by one-way ANOVA followed by Tukey's multiple comparison post-hoc test. * $P < 0.05$ vs. control; * * $P < 0.01$. C) Western-blot showing the induction of P-CAMKII upon treatment with 10 µM NNC, which is reversed by calcium signaling inhibitors. β-actin was used as a loading control. Plot (right) represents the quantification of P-CAMKII levels normalized against β-actin (n = 8). * $P < 0.05$ vs. control; #, $P < 0.05$ compared to NNC; ##, $P < 0.01$ compared to NNC.

fluorescence intensity (before treatment, F_0) and represented as the ratio F/F_0. As in most experiments control (untreated) cells experienced a progressive increase in F in lengthy measurements, we subtracted control F/F_0 from treatment F/F_0. Both graphs (non-subtracted and subtracted) are represented.

2.7. Apoptosis analysis

Annexin-V/PI staining experiments were performed after 24–36 h (A172 cells) or 48–60 h (primary cultures) of NNC 10 µM. Cells were trypsinized, washed in PBS, centrifuged (1 000 x g, 5 min) and combined with the cell culture supernatant. Cells were stained (15 min, room temperature) with Annexin-V-FITC (Immunotools) and PI (0.02 mg/ml). The % of apoptotic cells was evaluated using a FACS Canto II flow cytometer (BD Biosciences, USA). For each condition 20,000 cells were recorded in at least three independent experiments.

2.8. Cell viability assay

Cell viability was measured by the WST-1 (4-[3-(4-iodophenyl)-2-(4-nitrophenyl)-2H-5 tetrazolium]-1,3-benzene disulfonate) colorimetric assay. Cells were plated on 96-well plates (5000 cells/well), treated for 24 h, and then incubated for 60–120 min with 0.5 mg/ml WST-1 after 48 h of plating. Absorbance was measured at 440 nm using a reference filter at 620-nm wavelength in a microplate reader (Bio-Rad Laboratories). Assays were performed in at least three independent experiments, using triplicate measurements per condition.

2.9. Statistical analyses and ImageJ

Statistical significance was assessed by one-way ANOVA (Fig. 1B) or Student's t-test. Asterisks and hash signs represent different significance levels (*or # $P < 0.05$; **or ## $P < 0.01$; and *** or ### $P < 0.001$). Data is always represented as mean ± SEM. A Supplementary file including all the statistical parameters is included.

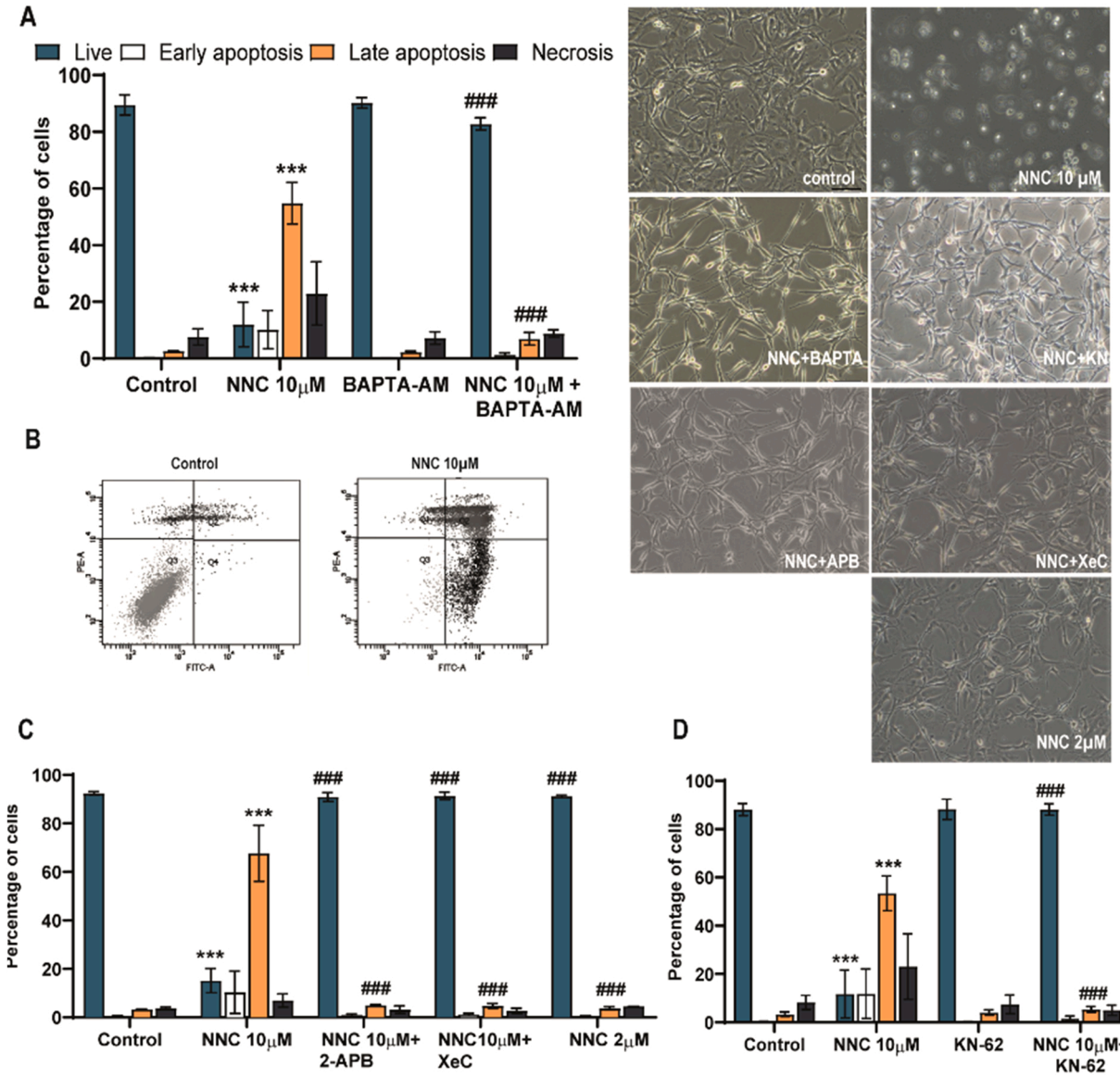

Fig. 2. Calcium signaling inhibitors rescue the cell death triggered by 10 μM NNC. A) Annexin-V/PI experiments were performed in A172 control cells, cells treated with 10 μM NNC, the calcium chelator BAPTA-AM (5 μM) or co-treated with BAPTA-AM and NNC. Right, plot represents the % of live cells and cells in early, late apoptosis or necrosis (n = 4). Left, representative phase contrast images of cell cultures after 36 h of incubation with the indicated drugs (bar= 100 μm). B) Examples of scatter plot of flow cytometry analysis for control and NNC-treated cultures. Y axis represents the PI fluorescence and the X axis the Annexin-V FITC fluorescence (Q1 represents necrosis, Q2 late apoptosis, Q3 live cells and Q4 early apoptosis). C) Annexin-V/PI experiments of control cells, cells treated with NNC (at the indicated concentration), the IP3R antagonists 2-APB (40 μM) and XeC (5 μM) or co-treated with NNC and the IP_3R antagonists (n = 3). D) Annexin-V/PI experiments of control cells, cells treated with NNC, the CAMKII inhibitor KN-62 (10 μM) or co-treated with KN-62 and NNC (n = 3). * ** , $P < 0.001$ compared to control; ###, $P < 0.001$ compared to NNC.

3. Results

3.1. The TTCC blocker NNC-55–0396 increases cytosolic calcium and activates calcium signaling cascades

We aimed at understanding the signaling mechanisms triggered by the TTCC blocker NNC55–0396 (hereafter NNC) that result in GBM cell death. First, we examined the concentration-dependence of NNC on A172 GBM cell viability by performing WST-1 assays. Data obtained indicated an IC_{50} of 4.8 μM NNC (Fig. 1A). Cell viability was only reduced by ~ 20% at 2 μM NNC, whereas it was severely compromised at 10 μM NNC (with a reduction of 80% of viable cells) after 24 h of treatment. This result was in agreement with the reported abrupt cell death of GBM cell lines induced by 10 μM NNC [11]. We next monitored cytosolic calcium levels in NNC-treated cells (at the cytotoxic concentration of 10 μM NNC and at 2 μM NNC, below the IC_{50}). Fluo-4 measurements showed a slow onset but sustained increase of calcium levels after addition of 10 μM NNC (Fig. 1B), which was not observed with 2 μM NNC. To investigate a possible calcium mobilization from the ER, the main calcium store of eukaryotic cells, we then co-applied NNC with the inositol-3-phosphate receptor (IP_3R) antagonists Xestospongin-C (XeC, 5 μM) or 2-Aminoethoxydiphenyl borate (2-APB, 40 μM [19–25]. 2-APB, and to a lesser extent XeC, minimized the increase in calcium levels triggered by NNC (Fig. 1B). Thus, unexpectedly, 10 μM NNC causes a persistent rise of cytosolic calcium levels in GBM cells by promoting calcium exit from the ER through IP_3R.

Calmodulin kinase-II (CAMKII) links ER stress and apoptosis [22]. We therefore analyzed the activation/phosphorylation of CAMKII after application of NNC alone or in combination with the calcium chelator BAPTA-AM (5 μM), the IP_3R antagonist 2-APB or with the selective

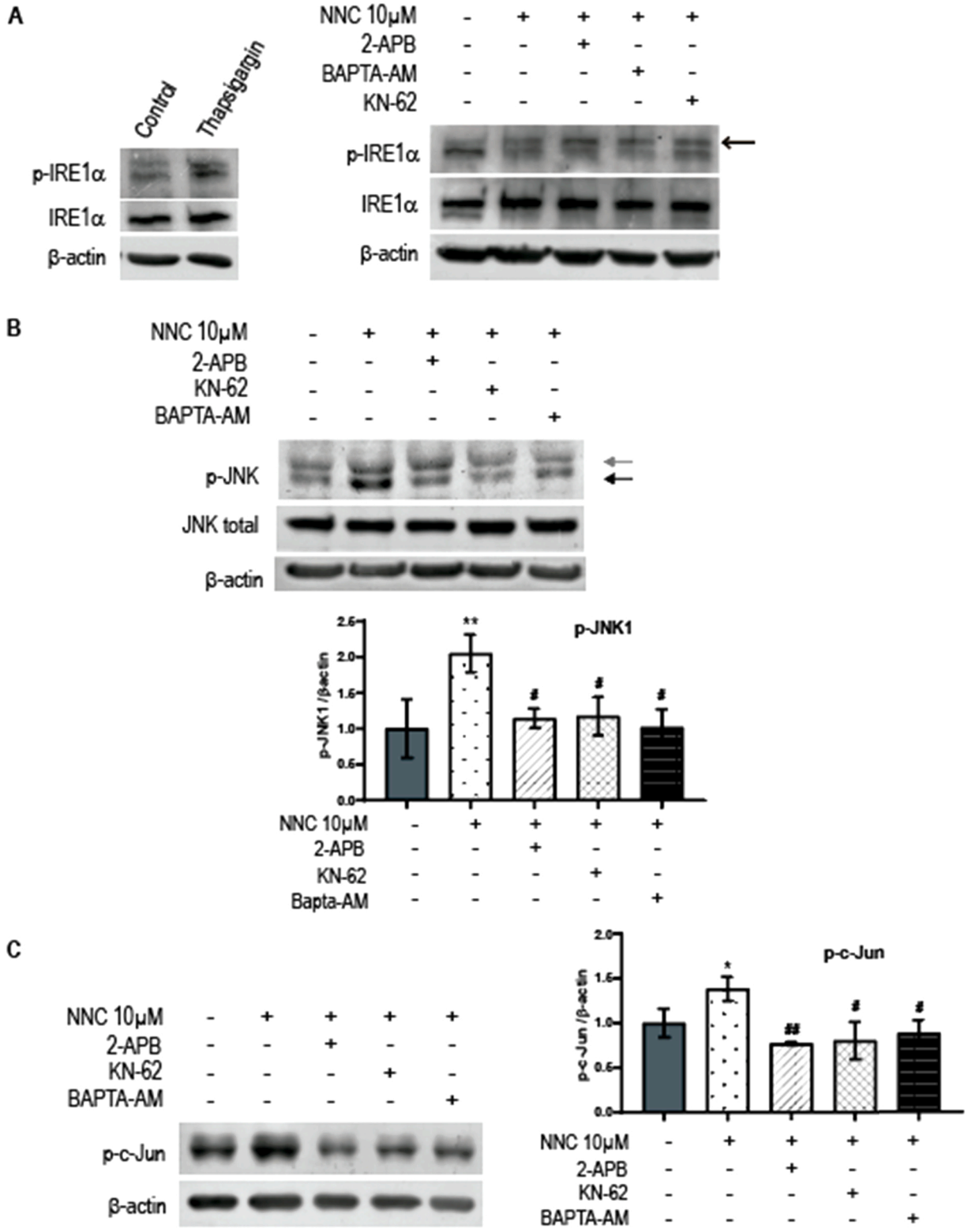

Fig. 3. NNC (10 μM) activates the IRE1α branch of the UPR. A) Tg (5 μM, 24 h), shown as a positive control, increases P-IRE1α levels (right). NNC-treated A172 cells (8 h) show increased intensity in a higher mobility band of P-IRE1α compared to untreated cells, while co-treatment with NNC and calcium signaling inhibitors do not change P-IRE1α upper band (arrow). IRE1α total levels do not change significantly. β-actin was used as a loading control. B) NNC-treated cells increase the lower mobility band of P-JNK (likely corresponding to P-JNK1; black arrow) compared to untreated cells. Co-treatment of NNC and calcium signaling inhibitors decreases P-JNK1 levels. JNK total levels do not change significantly. β-actin was used as a loading control. Plot represents the quantification of P-JNK1 levels normalized against β-actin (n = 6). C) P-c-jun, a known JNK target, was also analyzed by Western-blot. NNC-treated cells P-c-jun levels compared to untreated cells. Co-treatment of NNC and calcium signaling inhibitors decreases P-c-jun levels. β-actin was used as a loading control. Plot represents the quantification of P-c-jun levels normalized vs. β-actin (n = 3). * , $P < 0.05$ compared to control; ##, $P < 0.01$ compared to NNC; #, $P < 0.05$ compared to NNC.

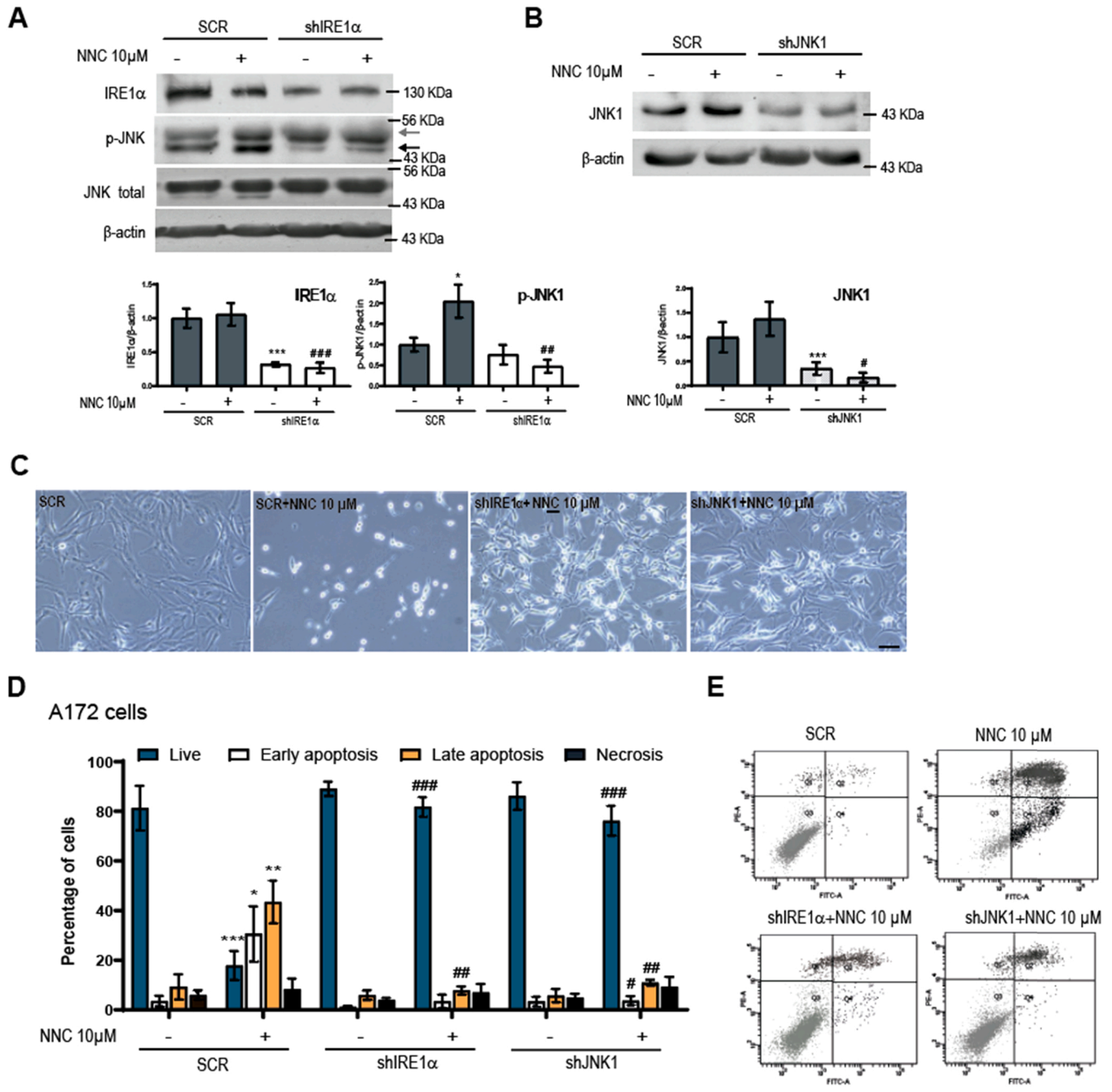

Fig. 4. Silencing IRE1α or JNK1 expression rescues NNC-triggered cell death. A172 cells expressing shRNA against *IRE1α* (A) and against JNK1 (B) compared to control cells (expressing scr shRNA) were treated with or without 10 μM NNC (8 h). The levels of IRE1α (A) and JNK1 (B) were significantly reduced (to approximately 30% as represented in the plots). Silencing *IRE1α* significantly reduces the activation of P-JNK1 (black arrow) detected by P-JNK antibodies and induced by NNC, while total JNK levels do not change. β-actin was used as a loading control. Plots represent the quantification the indicated levels normalized against β-actin (n = 4–7). C) Representative phase contrast images of control (scr) cells (untreated or treated with NNC) and cells silenced for IRE1α or JNK1 expression treated with NNC (10 μM, 36 h; bar =100 μm). D) Plot represents the % of live cells and cells in early, late apoptosis or necrosis obtained from Annexin-V/PI experiments (n = 5). Examples of flow cytometry analysis are shown at the bottom. Y axis represents the PI fluorescence and the X axis the Annexin-V FITC fluorescence. * , $P < 0.05$ compared to control; * *, $P < 0.01$ compared to control; * ** , $P < 0.001$ compared to control; #, $P < 0.05$ compared to NNC; ##, $P < 0.01$ compared to NNC; ###, $P < 0.001$ compared to NNC.

inhibitor of CAMKII KN-62 (10 μM), which blocks the binding of calcium-binding calmodulin to CAMKII [26,27]. NNC induced the phosphorylation of CAMKII at Thr286 ($P = 0.018$), which was reduced by the co-application of calcium signaling inhibitors (Fig. 1C; $P = 0.046$ for BAPTA-AM, $P = 0.016$ KN-62 and $P = 0.010$ for 2-APB).

To understand the relationship between the increase in cytosolic calcium and the induction of cell death, we tested whether lowering free cytosolic calcium would affect NNC-mediated effects. To this aim, we performed Annexin-V/Propidium iodine (PI) staining of A172 cells treated with NNC (10 μM, 36 h), alone or combined with the cell-permeable calcium chelator BAPTA-AM. NNC-treatment increased apoptosis ($P = 0.002$), whereas combining NNC with BAPTA-AM preserved cell viability (Fig. 2A and 2B; $P = 0.0003$). We also analyzed cells treated with 2 μM NNC, in which the % of cell death was as low as in untreated cells (Fig. 2C). Furthermore, the % of live cells in the co-treatments NNC plus the IP_3R antagonists were similar to the control

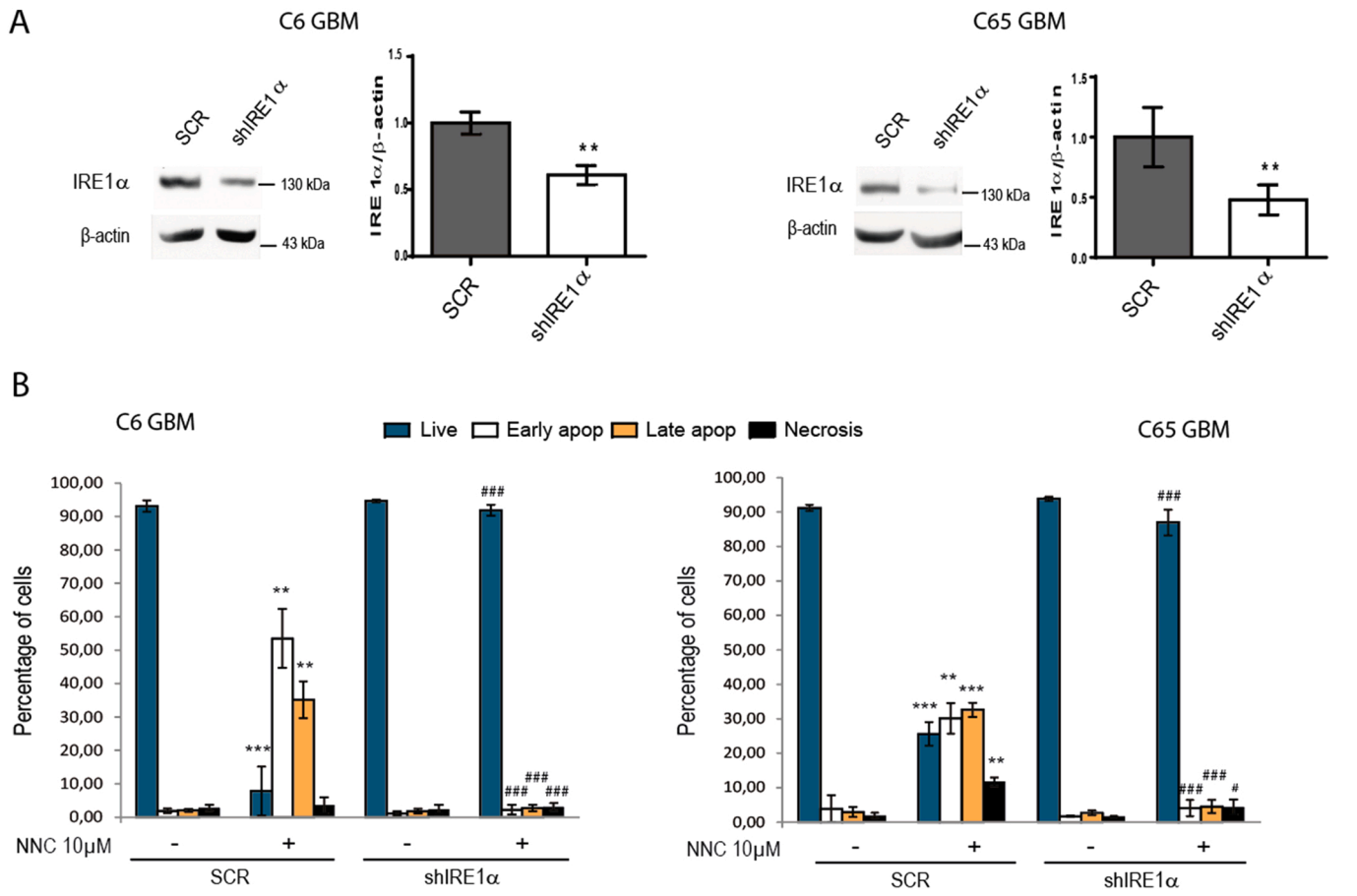

Fig. 5. Silencing *IRE1α* prevents the cell death triggered by NNC (10 μM) in two patient-derived GBM cultures. A) The levels of IRE1α were analyzed in control (scr cells) or cells expressing shRNA against IRE1α and quantified (normalized vs. β-actin, used as loading control). IRE1α levels were significantly reduced (to approximately 50% levels of scr cells). Two patient-derived GBM cultures were used, C6 and C65. B) Plot represents the % of live cells and cells in early, late apoptosis or necrosis obtained from Annexin-V/PI experiments in scr and shIRE1α GBM cultures (n = 3). * , $P < 0.05$; * *, $P < 0.01$; * ** , $P < 0.001$.

(Fig. 2C). KN-62 also rescued the GBM cell death triggered by NNC (Fig. 2D; $P = 0.0007$). These findings indicate that ER calcium mobilization and subsequent activation of CAMKII triggers the cell death response induced by NNC.

3.2. NNC activates IRE1α and JNK1 to promote cell death of GBM cells

ER calcium depletion through IP_3R and activation of CAMKII can promote UPR and cell death [26,28,29]. In our UPR analysis upon NNC treatment, we focused on the IRE1α branch because of its involvement in GBM development [6]. Western-blots of phosphorylated (P)-IRE1α showed an upper migrating IRE1α band in NNC-treated samples, also observed in Tg-treated cells but absent in control cell lysates, indicating IRE1α activation (Fig. 3 A). Samples obtained from A172 cells co-treated with NNC and the calcium signaling inhibitors (2-APB, KN-62) or the calcium chelator (BAPTA-AM) still displayed this band. In contrast, IRE1α total levels did not change significantly in any condition (Fig. 3A). These results indicate that IRE1α is activated by NNC regardless of inhibition of calcium efflux/signaling. Furthermore, we confirmed the IRE1α activation by NNC in two biopsy-derived GBM cultures (C6 and C65; Suppl. Fig. 1).

We additionally analyzed JNK as this kinase is a component of the IRE1α UPR branch and a critical mediator of apoptotic responses, including those mediated by CAMKII. We detected increased P-JNK levels in lysates from NNC-treated cells (specifically in the lower migrating band of the P-JNK doublet, corresponding to P-JNK1; $P = 0.0026$). Strikingly, P-JNK induction was significantly reduced when NNC was applied together with BAPTA-AM, 2-APB or KN-62 in A172 (Fig. 3B; $P = 0.02$, $P = 0.035$ and $P = 0.032$, respectively) and primary GBM cells (Suppl. Fig. 1). To confirm the activation of the JNK signaling pathway, we also analyzed the levels of P-c-jun, a JNK target. P-c-jun levels increased in NNC-treated cells ($P = 0.026$) and decreased when NNC was combined with the calcium inhibitors (Fig. 3C; $P = 0.005$, $P = 0.046$ and $P = 0.035$, respectively), in agreement with P-JNK results. These findings indicate that P-JNK1 plays a critical role in the cell death signaling cascade promoted by NNC, acting downstream of the ER calcium mobilization.

To check the involvement of IRE1α and JNK1 in the apoptotic response induced by NNC, we silenced both proteins and analyzed the cell death response to NNC by Annexin V/PI staining. We achieved a depletion of 50–70% in both proteins following the expression of shRNAs of *IRE1α* or *JNK1* compared to control cells (expressing scrambled shRNA; scr) in A172 cell line (Fig. 4A; $P < 0.00001$) and primary GBM cultures (Fig. 5 A; $P = 0.007$ and $P = 0.002$). Of note, silencing *IRE1α* significantly reduced the activation of p-JNK by NNC ($P = 0.006$), indicating that JNK is downstream of IRE1α (Fig. 4A; $P = 0.0019$). A172 cells expressing scr shRNA treated with NNC (10 μM) underwent apoptosis, as previously observed. On the contrary, the majority of A172 cells depleted of IRE1α or JNK1 challenged with NNC did not undergo apoptosis (Fig. 4D and E; $P = 0.0001$). Similar results were obtained in two primary GBM cultures depleted of IRE1α and challenged with NNC (Fig. 5B). Therefore, IRE1α and JNK1 activation are necessary for the GBM cell death promoted by NNC.

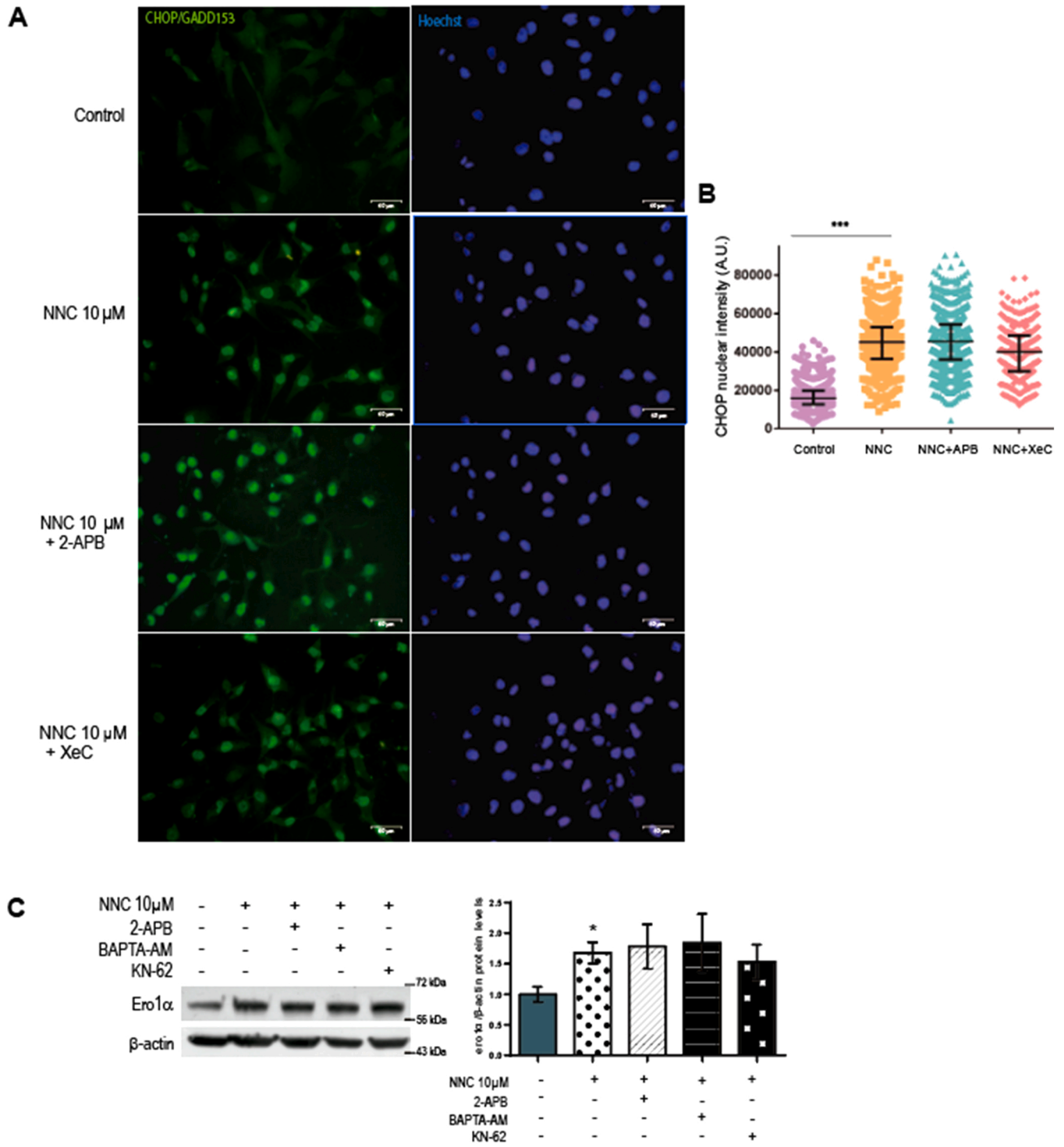

Fig. 6. NNC (10 μM) activates nuclear CHOP and increases the levels of its target, ERO1α. CHOP immunostaining was performed in untreated A172 cells, cells treated with 10 μM NNC or co-treated with NNC and the IP_3R antagonists XeC or 2-APB. Nuclear translocation of CHOP is observed in NNC-treated cells, regardless of the co-treatment with the IP_3R antagonists. Hoechst staining was used to show the nuclei. Bar= 50 μm. B) Quantification of the CHOP nuclear immunostaining from untreated cells or cells treated with NNC (alone or in combination with XeC or 2-APB). The intensity of CHOP nuclear immunostaining increases 2.8-fold upon NNC treatment and remains at this level in the co-treatments (> 200 cells were measured/experiment, n = 3; *** $P < 0.001$). C) ERO1α levels were analyzed from cell lysates of untreated A172 cells, treated with NNC alone or together with the calcium signaling inhibitors (2-APB, BAPTA-AM or KN-62). β-actin was used as a loading control. Plots show the quantification of ERO1α levels normalized against β-actin (n = 3). * , $P < 0.05$ compared to control. NNC increases ERO1 upstream of the calcium mobilization.

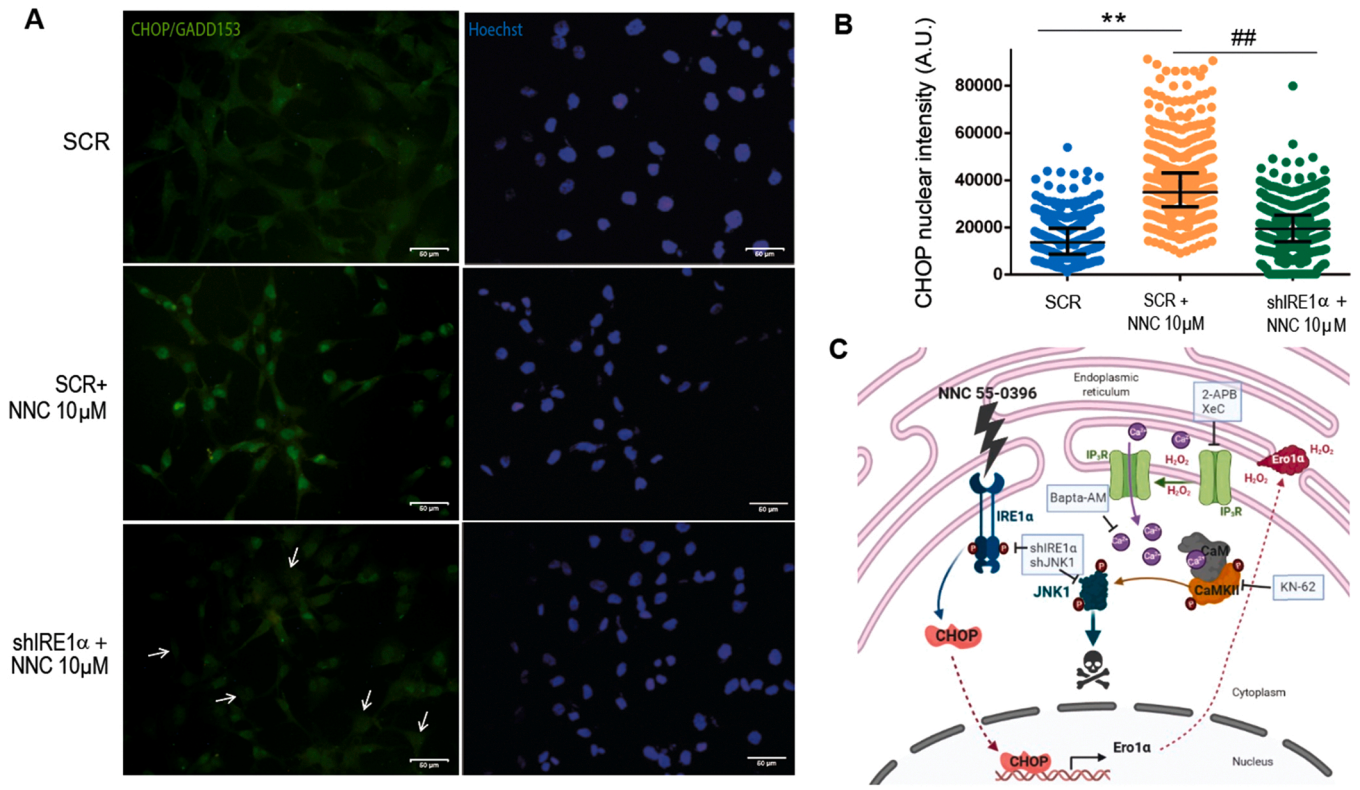

Fig. 7. NNC-mediated CHOP activation depends on IRE1α. A) Control (scr) and cells depleted of IRE1α (untreated or treated with 10 μM NNC) were immunostained for CHOP. CHOP nuclear translocation decreases in cells silenced for IRE1α expression. Hoechst staining is used to show the nuclei (arrows point to cells displaying low nuclear CHOP immunostaining); bar= 50 μm. B) Quantification of the CHOP nuclear immunostaining from control (scr) cells, scr cells treated with NNC and cells expressing the shRNA of IRE1α treated with NNC. The intensity of CHOP nuclear immunostaining is doubled by NNC treatment, while it returns to control values in cells depleted of IRE1α and treated with NNC (> 200 cells were measured/experiment, n = 4; ** $P < 0,05$ vs. SCR, and ## $P < 0,05$ vs. NNC). C) Proposed model: NNC activates IRE1α leading to CHOP nuclear translocation and activation, which increases ERO1α levels. This may promote an oxidant environment causing IP_3R activation and ER calcium efflux that in turn activates CAMKII and JNK1, leading to apoptosis.

3.3. CHOP/GADD153 links redox stress and apoptotic induction by NNC

Prolonged ER stress leads to cell death and CHOP is a central player of apoptosis downstream of the UPR. We investigated the possible involvement of CHOP in the NNC-dependent cell death. First, control and NNC-treated cells were immunostained for CHOP. The nuclear localization of CHOP was evident in NNC-treated cells (10 μM), indicating CHOP activation. In contrast, CHOP immunostaining remained weak and cytoplasmatic in control cells (Fig. 6A). Furthermore, cells co-treated with NNC and IP_3R antagonists (2-APB/XeC) still displayed nuclear CHOP (Fig. 6A and B).

CHOP can induce apoptosis through the regulation of its target ERO1α [27] that oxidizes the ER lumen during ER stress. Moreover, ERO1α activation is linked to IP_3R-calcium dependent apoptosis [28]. We found a significant elevation of ERO1α levels in NNC-treated cells ($P = 0.017$), which was maintained when NNC was combined with calcium signaling inhibitors (BAPTA-AM, KN-62 and 2-APB; Fig. 6C). These results relate ERO1α to the CHOP activation induced by NNC and implicate ERO1α in the feedback loop that emanates from the stressed ER, upstream of calcium mobilization. Additionally, while NNC-treated control cells showed strong nuclear CHOP signal, depletion of IRE1α reduced nuclear CHOP to control levels (Fig. 7A and B). These results involve CHOP in the apoptosis induced by NNC, downstream of IRE1α and upstream of the calcium mobilization/signaling (Fig. 7C).

4. Discussion

NNC-55–0396 was synthesized from mibefradil by replacing a methoxyacetylester with more lipophilic groups [29], being regarded as more selective against TTCCs. However, our work demonstrates that application of NNC to GBM cells -at a therapeutically relevant concentration of 10 μM- exerts cytotoxic effects by mobilizing ER calcium. This is necessarily an off-target effect, since: (1) block of plasma membrane calcium channels is bound to reduce cytosolic calcium levels; and (2) application of NNC at the lower, yet supramaximal concentration for TTCC block of 2 μM, does not elevate cytosolic calcium levels or induce cytotoxicity in GBM cells (but a moderate cytostatic effect at 24 h treatment). Previously, it had been shown that mibefradil at concentrations above 10 μM induced calcium mobilization from IP_3R-sensitive stores in rat cardiac fibroblasts and human platelets [30]. Our data show that the NNC-induced rise in cytosolic calcium can be mostly prevented by 2-APB, and to a lesser extent by XeC, which at the tested concentrations share the ability to inhibit IP_3R. Additionally, 2-APB has been reported to block Store-Operated Calcium Entry channels. Therefore, it could be concluded that both mechanisms are involved in calcium elevation by NNC, in syntony with the effects reported for mibefradil in different cell lines [31]. Importantly, NNC triggers GBM cell death by activating pro-apoptotic calcium signaling, as it is averted by the calcium chelator BAPTA-AM, CAMKII inhibitor KN-62, XeC or 2-APB. While XeC only prevents cytosolic calcium increase partially, it completely abrogates apoptosis. Thus, activation of IP_3Rs can be singled out as a necessary step towards NNC-induced cytotoxicity in GBM cells.

Our data also show that NNC-induced cell death relies on the dysregulation of the UPR. We had previously shown that mibefradil activates the UPR in melanoma cells [12] and cardiomyocytes [32]. Activation of IRE1α/CHOP by NNC occurs upstream of calcium release from the ER through IP_3R. Thus, IP_3R antagonists only reverse the induction of P-JNK1 and of P-c-Jun, which we place at a convergence

point between the IRE1α-dependent effects and the calcium signaling cascade emanating from the ER calcium exit (Fig. 7C). Interestingly, IRE1α can act both as a pro-survival and pro-death sensor, depending on the ER stress duration [33]. In fact, GBM cells display basally active IRE1α signaling, which favors tumor progression by remodeling the tumor stroma and inhibiting the immune response [6,34,35]. Consequently, small molecules with the ability to inhibit IRE1α activity have shown anti-tumor actions in vitro and in preclinical models [36]. Nonetheless, IRE1α hyperactivation leading to terminal UPR and ensuing apoptotic signaling might be an alternative strategy depending on cell type/context [36].

Here we show that NNC adds to the short list of known IRE1α activators and shRNA experiments demonstrate that the cytotoxicity of this compound is entirely based on this action. Overactivation of the IRE1α/CHOP/ERO1α axis can trigger oxidative stress [28] that results in calcium-dependent activation of JNK1. JNK1 has been shown to promote extrinsic and intrinsic apoptotic pathways, and to induce the expression of pro-apoptotic genes [37]. Autophagy could also play a role in cell-fate determination upon NNC treatment: IRE1α/JNK signaling is required for autophagy activation after ER stress [38]. Irrespective of the final execution pathway, hyperactivation of UPR in dying cancer cells favors the processing and presentation of tumor-associated antigens by dendritic cells to CD8 + cytotoxic T-cells [39], whose infiltration in GBM associates with longer survival [40]. Oxidative ER stress can trigger the release of Damage-associated Molecular Patterns, components of the innate immune response recognized by macrophages and other sentinel cells [41]. In addition, ATP is released by lysosomal exocytosis in dying cells [42], acting as a chemoattractant for microglia [43]. Altogether, NNC-mediated cell death is assumed as highly immunogenic.

An unresolved question is what is the primary target of NNC leading to IRE1α activation. While preventing cell death, chelation of cytosolic calcium, preclusion of ER calcium mobilization or inhibition of CAMKII do not decrease NNC-mediated IRE1α activation. These data place IP_3R activation downstream of IRE1α and discard that IRE1α activation is due to actions attributed to tetralol derivatives such as an agonist action on TrpM7 [44], the activation of Store-Operated Calcium Entry [31,45] or lysosomal permeabilization [46].

5. Conclusions

We report that application of NNC to GBM cell lines and biopsy-derived cultures triggers a terminal UPR, characterized by IRE1α activation and subsequent calcium mobilization through IP_3R, ultimately resulting in cell death. Thus, tetralols are disclosed as agents with multiple anticancer activities that add to their known blocking actions on TTCCs.

CRediT authorship contribution statement

All authors have read the manuscript. **AV**, designed and performed experiments, analyzed data, discussed results and revised the manuscript. **LA**, performed experiments, analyzed data and discussed results. **CA**, designed the project, analyzed data, received funding, discussed results and wrote the manuscript. **JH**, designed the project, analyzed data, received funding, discussed results and wrote the manuscript.

Conflict of interest statement

The authors declare no conflict of interest.

Data availability

Data will be made available on request.

Acknowledgements

We are grateful to Dr. S. Shaikh for help with initial calcium experiments and to Dr. E. Vilaprinyó for statistical analysis. We acknowledge the technical support of D. Argilés and assistance from the personnel of the Cell Culture and the Flow Cytometry Services of IRBLleida/UdL. This work was funded by grants from the Spanish Ministry of Science and Innovation/FEDER "Una manera de hacer Europa" (Retos Program, number RTI2018-094739-B-I00 to JH & CC) and Fundació La Marató de TV3 (number 235/C/2019 to CC). AV was funded by UdL, IRBLleida-Diputació de Lleida and La Marató de TV3. LA is a recipient of an FI-AGAUR predoctoral fellowship. Work supported by IRBLleida Biobank (B.0000682) and Plataforma Biobancos PT17/0015/0027/.

Appendix A. Supporting information

Supplementary data associated with this article can be found in the online version at doi:10.1016/j.biopha.2022.112881.

References

[1] J. Obacz, T. Avril, P.J. Le Reste, H. Urra, V. Quillien, C. Hetz, E. Chevet, Endoplasmic reticulum proteostasis in glioblastoma - From molecular mechanisms to therapeutic perspectives, Sci. Signal. 10 (2017) 1–19, https://doi.org/10.1126/scisignal.aal2323.

[2] C. Hetz, K. Zhang, R.J. Kaufman, Mechanisms, regulation and functions of the unfolded protein response, Nat. Rev. Mol. Cell Biol. 21 (2020) 421–438, https://doi.org/10.1038/s41580-020-0250-z.

[3] E. Madden, S.E. Logue, S.J. Healy, S. Manie, A. Samali, The role of the unfolded protein response in cancer progression: from oncogenesis to chemoresistance, Biol. Cell. 111 (2019) 1–17, https://doi.org/10.1111/boc.201800050.

[4] R.P. Junjappa, P. Patil, K.R. Bhattarai, H.R. Kim, H.J. Chae, IRE1α implications in endoplasmic reticulum stress-mediated development and pathogenesis of autoimmune diseases, Front. Immunol. 9 (2018), https://doi.org/10.3389/fimmu.2018.01289.

[5] C. Greenman, P. Stephens, R. Smith, G.L. Dalgliesh, C. Hunter, G. Bignell, H. Davies, J. Teague, A. Butler, S. Edkins, S.O. Meara, I. Vastrik, E.E. Schmidt, T. Avis, S. Barthorpe, G. Bhamra, G. Buck, B. Choudhury, J. Clements, J. Cole, E. Dicks, S. Forbes, K. Gray, K. Halliday, R. Harrison, K. Hills, J. Hinton, A. Jenkinson, D. Jones, A. Menzies, J. Perry, K. Raine, D. Richardson, R. Shepherd, A. Small, C. Tofts, J. Varian, T. Webb, S. West, S. Widaa, A. Yates, D.P. Cahill, D. N. Louis, P. Goldstraw, A.G. Nicholson, F. Brasseur, L. Looijenga, B.L. Weber, Y. Chiew, M.F. Greaves, A.R. Green, P. Campbell, E. Birney, F. Douglas, Patterns of somatic mutation in human cancer genomes, Nature 446 (2007) 153–158, https://doi.org/10.1038/nature05610.Patterns.

[6] S. Lhomond, T. Avril, N. Dejeans, K. Voutetakis, D. Doultsinos, M. McMahon, R. Pineau, J. Obacz, O. Papadodima, F. Jouan, H. Bourien, M. Logotheti, G. Jégou, N. Pallares-Lupon, K. Schmit, P. Le Reste, A. Etcheverry, J. Mosser, K. Barroso, E. Vauléon, M. Maurel, A. Samali, J.B. Patterson, O. Pluquet, C. Hetz, V. Quillien, A. Chatziioannou, E. Chevet, Dual IRE 1 RNase functions dictate glioblastoma development, EMBO Mol. Med. 10 (2018) 1–19, https://doi.org/10.15252/emmm.201707929.

[7] N.M. Peñaranda Fajardo, C. Meijer, F.A.E. Kruyt, The endoplasmic reticulum stress/unfolded protein response in gliomagenesis, tumor progression and as a therapeutic target in glioblastoma, Biochem. Pharmacol. 118 (2016) 1–8, https://doi.org/10.1016/j.bcp.2016.04.008.

[8] D.M. Rodman, K. Reese, J. Harral, B. Fouty, S. Wu, J. West, M. Hoedt-Miller, Y. Tada, K.X. Li, C. Cool, K. Fagan, L. Cribbs, Low-voltage-activated (T-type) calcium channels control proliferation of human pulmonary artery myocytes, Circ. Res. 96 (2005) 864–872, https://doi.org/10.1161/01.RES.0000163066.07472.ff.

[9] J.A. Rodríguez-Gómez, K.L. Levitsky, J. López-Barneo, T-type Ca2+ channels in mouse embryonic stem cells: modulation during cell cycle and contribution to self-renewal, Am. J. Physiol. Cell Physiol. 302 (2012) C494–C504, https://doi.org/10.1152/ajpcell.00267.2011.

[10] M.C. Sallan, A. Visa, S. Shaikh, M. Nager, J. Herreros, C. Cantí, T-type Ca2+ Channels: T for targetable, Cancer Res. 78 (2018) 603–609, https://doi.org/10.1158/0008-5472.CAN-17-3061.

[11] A. Visa, M.C. Sallan, O. Maiques, L. Alza, E. Talavera, R. Lopez-Ortega, M. Santacana, J. Herreros, C. Cantí, T-type Cav3.1 channels mediate progression and chemotherapeutic resistance in glioblastoma, Cancer Res. 79 (2019) 1857–1868, https://doi.org/10.1158/0008-5472.CAN-18-1924.

[12] A. Das, C. Pushparaj, J. Herreros, M. Nager, R. Vilella, M. Portero, R. Pamplona, X. Matias-Guiu, R.M. Martí, C. Cantí, T-type calcium channel blockers inhibit autophagy and promote apoptosis of malignant melanoma cells, Pigment Cell Melanoma Res. 26 (2013) 874–885, https://doi.org/10.1111/pcmr.12155.

[13] J.P. Sheehan, Z. Xu, B. Popp, L. Kowalski, D. Schlesinger, Inhibition of glioblastoma and enhancement of survival via the use of mibefradil in conjunction with radiosurgery, J. Neurosurg. 118 (2013) 830–837, https://doi.org/10.3171/2012.11.JNS121087.

[14] S.T. Keir, H.S. Friedman, D.A. Reardon, D.D. Bigner, L.A. Gray, Mibefradil, a novel therapy for glioblastoma multiforme: Cell cycle synchronization and interlaced therapy in a murine model, J. Neurooncol. 111 (2013) 97–102, https://doi.org/10.1007/s11060-012-0995-0.
[15] K.H. Kim, D. Kim, J.Y. Park, H.J. Jung, Y.H. Cho, H.K. Kim, J. Han, K.Y. Choi, H. J. Kwon, NNC 55-0396, a T-type Ca2+ channel inhibitor, inhibits angiogenesis via suppression of hypoxia-inducible factor-1α signal transduction, J. Mol. Med. 93 (2015) 499–509, https://doi.org/10.1007/s00109-014-1235-1.
[16] M. Holdhoff, X. Ye, J.G. Supko, L.B. Nabors, A.S. Desai, T. Walbert, G.J. Lesser, W. L. Read, F.S. Lieberman, M.A. Lodge, J. Leal, J.D. Fisher, S. Desideri, S. A. Grossman, R.L. Wahl, D. Schiff, Timed sequential therapy of the selective T-type calcium channel blocker mibefradil and temozolomide in patients with recurrent high-grade gliomas, Neuro Oncol. 19 (2017) 845–852, https://doi.org/10.1093/neuonc/nox020.
[17] A. Visa, S. Shaikh, L. Alza, J. Herreros, C. Cantí, The hard-to-close window of T-type calcium channels, Trends Mol. Med. 25 (2019) 571–584, https://doi.org/10.1016/j.molmed.2019.03.001.
[18] M. Nàger, M.C. Sallán, A. Visa, C. Pushparaj, M. Santacana, A. Macià, A. Yeramian, C. Cantí, J. Herreros, Inhibition of WNT-CTNNB1 signaling upregulates SQSTM1 and sensitizes glioblastoma cells to autophagy blockers, Autophagy (2018) 1–18, https://doi.org/10.1080/15548627.2017.1423439.
[19] J. Gafni, J.A. Munsch, T.H. Lam, M.C. Catlin, L.G. Costa, T.F. Molinski, I.N. Pessah, Xestospongins: potent membrane permeable blockers of the inositol 1,4,5-trisphosphate receptor, Neuron 19 (1997) 723–733, https://doi.org/10.1016/S0896-6273(00)80384-0.
[20] T. Maruyama, T. Kanaji, S. Nakade, T. Kanno, K. Mikoshiba, 2APB, 2-aminoethoxydiphenyl borate, a membrane-penetrable modulator of Ins(l,4,5)P3-induced Ca2+ release, J. Biochem. 122 (1997) 498–505, https://doi.org/10.1093/oxfordjournals.jbchem.a021780.
[21] Y. Dobrydneva, P. Blackmore, 2-Aminoethoxydiphenyl borate directly inhibits store-operated calcium entry channels in human platelets, Mol. Pharmacol. 60 (2001) 541–552.
[22] J.M. Timmins, L. Ozcan, T.A. Seimon, G. Li, C. Malagelada, J. Backs, T. Backs, R. Bassel-Duby, E.N. Olson, M.E. Anderson, I. Tabas, Calcium/calmodulin-dependent protein kinase II links ER stress with Fas and mitochondrial apoptosis pathways, J. Clin. Investig. 119 (2009) 2925–2941, https://doi.org/10.1172/JCI38857.
[23] M. Terasawa, H. Hidaka, J.B. Chem, KN-62, a specific inhibitor of Ca2 +/Calmodulin-dependent Protein Kinase II *, J. Biol. Chem. 265 (1990) 4315–4320.
[24] K. Hübner, L. Phi-van, KN-62, a selective inhibitor of Ca2+/calmodulin-dependent protein kinase II, inhibits the lysozyme pre-mRNA splicing in myelomonocytic HD11 cells, Biochem. Biophys. Res. Commun. 319 (2004) 405–409, https://doi.org/10.1016/j.bbrc.2004.05.002.
[25] S. Kiviluoto, T. Vervliet, H. Ivanova, J.P. Decuypere, H. De Smedt, L. Missiaen, G. Bultynck, J.B. Parys, Regulation of inositol 1,4,5-trisphosphate receptors during endoplasmic reticulum stress, Biochim. Biophys. Acta Mol. Cell Res. 1833 (2013) 1612–1624, https://doi.org/10.1016/j.bbamcr.2013.01.026.
[26] I. Tabas, D. Ron, Integrating the mechanisms of apoptosis induced by endoplasmic reticulum stress, Nat. Cell Biol. 13 (2011) 184–190, https://doi.org/10.1038/jid.2014.371.
[27] S.J. Marciniak, C.Y. Yun, S. Oyadomari, I. Novoa, Y. Zhang, R. Jungreis, K. Nagata, H.P. Harding, D. Ron, CHOP induces death by promoting protein synthesis and oxidation in the stressed endoplasmic reticulum, Genes Dev. 18 (2004) 3066–3077, https://doi.org/10.1101/gad.1250704.
[28] G. Li, M. Mongillo, K.T. Chin, H. Harding, D. Ron, A.R. Marks, I. Tabas, Role of ERO1-α-mediated stimulation of inositol 1,4,5-triphosphate receptor activity in endoplasmic reticulum stress-induced apoptosis, J. Cell Biol. 186 (2009) 783–792, https://doi.org/10.1083/jcb.200904060.
[29] M. Li, J.B. Hansen, L. Huang, B.M. Keyser, J.T. Taylor, Towards selective antagonists of T-type calcium channels: design, characterization and potential applications of NNC 55-0396, Cardiovasc. Drug Rev. 23 (2005) 173–196.
[30] M. Eberhard, K. Miyagawa, K. Hermeyer, P. Erne, Effects of mibefradil on intracellular Ca2+ release in cultured rat cardiac fibroblasts and human platelets, Naunyn Schmiede Arch. Pharmacol. 353 (1995) 94–101, https://doi.org/10.1007/BF00168921.
[31] G.H.S. Bomfim, E. Mitaishvili, T.F. Aguiar, R.S. Lacruz, Mibefradil alters intracellular calcium concentration by activation of phospholipase C and IP 3 receptor function, Mol. Biomed. 2 (2021).
[32] C. Pushparaj, A. Das, R. Purroy, M. Nàger, J. Herreros, R. Pamplona, C. Cantí, Voltage-gated calcium channel blockers deregulate macroautophagy in cardiomyocytes, Int. J. Biochem. Cell Biol. 68 (2015) 166–175, https://doi.org/10.1016/j.biocel.2015.09.010.
[33] Y. Chen, F. Brandizzi, IRE1: ER stress sensor and cell fate executor, Trends Cell Biol. 23 (2013) 547–555, https://doi.org/10.1016/j.tcb.2013.06.005.
[34] C. Rubio-Patiño, J.P. Bossowski, E. Chevet, J.-E. Ricci, Reshaping the immune tumor microenvironment through IRE1 signaling, Trends Mol. Med. 24 (2018) 607–614, https://doi.org/10.1016/j.molmed.2018.05.005.
[35] J.J. Rodvold, S. Xian, J. Nussbacher, B. Tsui, T. Cameron Waller, S.C. Searles, A. Lew, P. Jiang, I. Babic, N. Nomura, J.H. Lin, S. Kesari, H. Carter, M. Zanetti, IRE1α and IGF signaling predict resistance to an endoplasmic reticulum stress-inducing drug in glioblastoma cells, Sci. Rep. 10 (2020) 8348, https://doi.org/10.1038/s41598-020-65320-6.
[36] D.P. Raymundo, D. Doultsinos, X. Guillory, A. Carlesso, L.A. Eriksson, E. Chevet, Pharmacological targeting of IRE1 in cancer, Trends Cancer 6 (2020) 1018–1030, https://doi.org/10.1016/j.trecan.2020.07.006.
[37] D.N. Dhanasekaran, E.P. Reddy, JNK-signaling: a multiplexing hub in programmed cell death, Genes Cancer 8 (2017) 682–694, https://doi.org/10.18632/genesandcancer.155.
[38] M. Ogata, S. Hino, A. Saito, K. Morikawa, S. Kondo, S. Kanemoto, T. Murakami, M. Taniguchi, I. Tanii, K. Yoshinaga, S. Shiosaka, J.A. Hammarback, F. Urano, K. Imaizumi, Autophagy is activated for cell survival after endoplasmic reticulum stress, Mol. Cell. Biol. 26 (2006) 9220–9231, https://doi.org/10.1128/MCB.01453-06.
[39] G. Kroemer, L. Galluzzi, Autophagy-dependent danger signaling and adaptive immunity to poorly immunogenic tumors, Oncotarget 8 (2017) 5686–5691, https://doi.org/10.18632/oncotarget.13892.
[40] J. Lohr, T. Ratliff, A. Huppertz, Y. Ge, C. Dictus, R. Ahmadi, S. Grau, N. Hiraoka, V. Eckstein, R.C. Ecker, T. Korff, A. von Deimling, A. Unterberg, P. Beckhove, C. Herold-Mende, Effector T-cell infiltration positively impacts survival of glioblastoma patients and is impaired by tumor-derived TGF-β, Clin. Cancer Res. 17 (2011) 4296–4308, https://doi.org/10.1158/1078-0432.CCR-10-2557.
[41] A.D. Garg, L. Galluzzi, L. Apetoh, T. Baert, R.B. Birge, J.M. Bravo-San Pedro, K. Breckpot, D. Brough, R. Chaurio, M. Cirone, A. Coosemans, P.G. Coulie, D. De Ruysscher, L. Dini, P. de Witte, A.M. Dudek-Peric, A. Faggioni, J. Fucikova, U. S. Gaipl, J. Golab, M.-L. Gougeon, M.R. Hamblin, A. Hemminki, M. Herrmann, J. W. Hodge, O. Kepp, G. Kroemer, D.V. Krysko, W.G. Land, F. Madeo, A.A. Manfredi, S.R. Mattarollo, C. Maueroder, N. Merendino, G. Multhoff, T. Pabst, J.-E. Ricci, C. Riganti, E. Romano, N. Rufo, M.J. Smyth, J. Sonnemann, R. Spisek, J. Stagg, E. Vacchelli, P. Vandenabeele, L. Vandenberk, B.J. Van den Eynde, S. Van Gool, F. Velotti, L. Zitvogel, P. Agostinis, Molecular and translational classifications of DAMPs in immunogenic cell death, Front. Immunol. 6 (2015) 588, https://doi.org/10.3389/fimmu.2015.00588.
[42] Y. Wang, I. Martins, Y. Ma, O. Kepp, L. Galluzzi, G. Kroemer, Autophagy-dependent ATP release from dying cells via lysosomal exocytosis, Autophagy 9 (2013) 1624–1625, https://doi.org/10.4161/auto.25873.
[43] Y. Fan, L. Xie, C.Y. Chung, Signaling pathways controlling microglia chemotaxis, Mol. Cells 40 (2017) 163–168, https://doi.org/10.14348/molcells.2017.0011.
[44] S. Schäfer, S. Ferioli, T. Hofmann, S. Zierler, T. Gudermann, V. Chubanov, Mibefradil represents a new class of benzimidazole TRPM7 channel agonists, Pflüg. Arch. Eur. J. Physiol. 468 (2016) 623–634, https://doi.org/10.1007/s00424-015-1772-7.
[45] M.T. Johnson, A. Gudlur, X. Zhang, P. Xin, S.M. Emrich, R.E. Yoast, R. Courjaret, R. M. Nwokonko, W. Li, N. Hempel, K. Machaca, D.L. Gill, P.G. Hogan, M. Trebak, L-type calcium channel blockers promote vascular remodeling through activation of STIM proteins, Proc. Natl. Acad. Sci. USA 117 (2020) 17369 LP–17380, https://doi.org/10.1073/pnas.2007598117.
[46] J.C. Chávez, J.L. De la Vega-Beltrán, O. José, P. Torres, T. Nishigaki, C.L. Treviño, A. Darszon, Acrosomal alkalization triggers Ca(2+) release and acrosome reaction in mammalian spermatozoa, J. Cell. Physiol. 233 (2018) 4735–4747, https://doi.org/10.1002/jcp.26262.